Journal of Vibration Engineering & Technologies (2024) 12:5203–5218
https://doi.org/10.1007/s42417-023-01192-0

ORIGINAL PAPER

Effect of Functionally Graded Carbon Nanotube Reinforcement on the Dynamic Response of Composite Beams Subjected to a Moving Charge

İsmail Esen[1] · **Mehmet Akif Koç**[2] · **Mustafa Eroğlu**[3]

Received: 25 August 2023 / Revised: 3 October 2023 / Accepted: 11 October 2023 / Published online: 16 November 2023

Abstract

Purpose This article examines the forced vibrations of composite beams that have been reinforced with single-walled carbon nanotubes (SWCNTs) and subjected to a moving charge without considering the effect of mass inertia.

Methods This study investigates three different beams, namely uniform distribution carbon nanotubes (UD-CNT), functionally graded Λ distribution carbon nanotubes (FGΛ-CNT), and functionally graded X distribution carbon nanotubes (FGX-CNT). The SWCNTs exhibit length alignment along the axial direction, while their volume distributions are observed in the thickness direction. The motion equations of beams are derived using Hamilton's principle and mass interaction forces based on a sinusoidal third-order shear deformation theory (TSDT). These equations are then converted into a single equation set and solved using Navier's method.

Results This study presents comprehensive findings on the effects of total volume fraction and distribution types of carbon nanotubes (CNTs) on the forced vibration of a composite beam caused by a moving charge at different mass velocities. The FGX-CNT distribution of the beam has demonstrated increased resistance to the dynamic impact of live load.

Conclusion The study's findings will aid in the development of micro-sensors that carry moving charges.

Keywords FG-CNT reinforced composite beams · Third order beam theory · Navier method · Moving charge

Introduction

Extensive research has been conducted on advanced composites, specifically carbon nanotube (CNT) reinforced composites. These composites have gained attention due to their favorable electrical, thermal, and mechanical properties. The research has been driven by the need to address failure issues commonly observed in traditional laminated composites, such as delamination and micro defects. Extensive research has been conducted on advanced composites, specifically carbon nanotube (CNT) reinforced composites. This is due to their advantageous electrical, thermal, and mechanical properties, which make them a promising alternative to classical laminated composites. The motivation for this research stems from the failure problems caused by delamination and micro defects in the latter. Shen [1] has recently applied the concept of material gradation to nanocomposites in CNT-reinforced composite plates. Bohlen and Bolton [2] observed through molecular dynamics (MD) simulations that the Young's modulus of the composite beams is enhanced in the specified direction by the presence of aligned carbon nanotubes (CNTs). The accuracy of the general mixture rule for single-walled carbon nanotubes (SWCNT) has been challenged by [3]. As a result, [4] proposed an extended rule of mixture. The precise measurement of the effective wall thickness of the single-walled carbon nanotube (SWCNT) has been conducted by reference [5], and the accurate determination of the mechanical properties of the SWCNT has

✉ Mustafa Eroğlu
mustafaeroglu@sakarya.edu.tr

İsmail Esen
iesen@karabuk.edu.tr

Mehmet Akif Koç
makoc@subu.edu.tr

[1] Engineering Faculty, Mechanical Engineering Department, Karabük University, 78050 Karabük, Turkey

[2] Technology Faculty, Mechatronics Engineering Department, Sakarya Applied Sciences University, 54187 Sakarya, Turkey

[3] Engineering Faculty, Mechanical Engineering Department, Sakarya University, 54187 Sakarya, Turkey

been achieved. Additionally, previous studies [6, 7] have confirmed the mechanical properties of single-walled carbon nanotubes (SWCNTs) by applying the finite element method. Yas and Samadi [8] examined the buckling and free vibration characteristics of Timoshenko beams embedded with FG-CNTs. In their study, [9] investigated the capabilities of a novel RVE builder in constructing representative volume elements (RVEs) for CNT/Al composites. The RVE builder effectively created RVEs with high-volume fractions and intricate geometries of CNTs. Lin and Xiang [10] employed the First-order Shear Deformation Theory (FSDT) and the Third-order Shear Deformation Theory (TSDT) to investigate the natural frequency characteristics of composite beams made of Functionally Graded Carbon Nanotubes (FG-CNTs). The forced response of FG-CNT beams was investigated by Ansari et al. [11] using the first-order shear deformation theory (FSDT). A method referred to as [12] is utilized to measure the resistivity between individual carbon nanotubes (CNTs) and carbon black nanoparticles (CB NPs). Subsequently, an electrical model based on modified location analysis is employed to evaluate the piezoresistive properties of hybrid CNT-CB polymer nanocomposites when subjected to tension. Kee et al. synthesized a polyamide nanocomposite containing multi-walled carbon nanotubes (MWCNT) and EG network structures using supercritical CO_2 [13]. Aydogdu [14] investigated the vibration response of composite beams made of functionally graded carbon nanotubes (FG-CNT) using various time-stepping differential transformation methods (TSDT). The nonlinear forced response of FG-CNT beams has been investigated in previous studies [11, 15] using the Timoshenko beam theory (TBT) and considering von Kármán geometric nonlinearity. Shahmohammadi et al. [16] investigated the nonlinear response of FG-CNT under in-plane and lateral loads. Chaudhari and Lal [17] investigated the free vibration behavior of elastically supported beams made of functionally graded carbon nanotubes (FG-CNT) under varying temperature conditions. Saffari et al. studied functionally graded carbon nanotube-reinforced composite sandwich nanoplate free vibration in a longitudinal magnetic field [18]. Wu et al. [19] investigated the post-buckling response of composite beams made of functionally graded carbon nanotube (FG-CNT) materials under varying temperature conditions. Gholami et al. [20] employed the Timoshenko beam theory to investigate the dynamic behavior of FG-CNT composite beams with geometric defects under harmonic transverse loads. Shafiei and Setoodeh [21] assessed the post-buckling and free vibration characteristics of beams made of functionally graded carbon nanotube (FG-CNT) material on a nonlinear base. Ghorbani et al. [22] investigated the thermal vibration characteristics of pre-twisted beams made of functionally graded carbon nanotube (FG-CNT) materials. Vo-Duy et al. [23] investigated the free vibration characteristics of composite beams made of functionally graded carbon nanotube (FG-CNT) materials. They employed a novel Timoshenko shear deformation theory (TSDT) combined with a finite element method for their analysis. Khosravi et al. [24] investigated the vibrational characteristics of spinning FG-CNTs in a temperature-controlled setting. Wu et al. [25] investigated the resonances of FG-CNT composite beams, including both fundamental and superharmonic resonances. Taş and Soykok [26] examined the impact of incorporating CNTs on the stiffness of composite beams. Talebizadehsardari et al. [27] examined the static bending characteristics of curved beams made of functionally graded carbon nanotubes (FG-CNT). Khosravi et al. [28] conducted a thermal buckling analysis of spinning beams made of functionally graded carbon nanotube (FG-CNT) material using the First-order Shear Deformation Theory (FSDT). Garcia et al. [29] investigated the modeling of performance characteristics and elastic moduli of polymer composites reinforced with carbon nanotubes (CNTs). Ahmadi et al. [30] investigated the behavior of polymer beams reinforced with carbon nanotubes (CNTs) when subjected to low velocity impact. They employed a hierarchical finite element approach for their study. Ranjbar et al. [31] investigated the low-velocity impact behavior of axially loaded beams made of functionally graded carbon nanotubes (FG-CNTs). Fallah et al. [32] proposed a semi-exact solution technique for analyzing the nonlinear dynamics of functionally graded carbon nanotubes (FG-CNTs) beams. Fadaee et al. [33] examined the dynamic stability of a spinning FG-CNT with a magnetorheological elastomer core. Palacios and Ganesan [34] investigated the dynamic response of polymer materials reinforced with carbon nanotubes (CNTs) through a multiscale finite element analysis. In their study, Fu et al. [35] examined the mechanical behavior of laminated plates reinforced with carbon nanotubes (CNTs) under heat loads. The plates were also supported on elastic foundations. Kamarian et al. [36] investigated the influence of carbon nanotubes (CNTs) on the thermal buckling behavior of rectangular laminated composite plates. Tran et al. [37] analyzed the static behavior of smart laminated and carbon nanotube (CNT)-reinforced composite plates. They employed a novel four-variable plate theory for this purpose. In their study, Di Sciuva and Sorrenty [38] investigated the behavior of FG-CNT sandwich plates regarding free vibration, bending, and buckling. The Zigzag Theory was employed for this analysis. Uspensky et al. designed a sandwich cylindrical shell with a honeycomb core and carbon nanotube-reinforced composite surface layers [39]. Chitour et al. [40] investigated the bending behavior of sandwich plate constructions with functional gradations under sinusoidal loads. The study by Reference [41] thoroughly analyzed the outcomes of 2D-FG sandwich porous plates of varying thicknesses. Bouazza and Zenkour employed an enhanced nth-higher-order theory to analyze

the vibration characteristics of plates reinforced with carbon nanotubes (CNTs) [42]. Adıyaman analyzes free vibration in a 2D porous functionally graded beam [43]. To strengthen composite plates using functionally graded carbon nanotubes (FG-CNTs), Uymaz et al. undertook a three-dimensional thermal vibration study [44]. Civalek and Jalaei [45] examined the shear buckling behavior of skew plates reinforced with carbon nanotubes (CNTs). Taati et al. [46] developed a semi-analytical solution for the nonlinear vibration of beams reinforced with carbon nanotubes (CNTs), accounting for shear and small-scale effects. Sobhy [47] utilized the Levy solution to examine the response of plates reinforced with carbon nanotubes (CNTs) subjected to different distributed loads. Yuan et al. [48] examine the vibration analysis of viscoelastic nanobeams reinforced with functionally graded carbon nanotubes (FG-CNTs) under magneto-hygro-thermal loading, based on a sinusoidal high-order shear deformation theory. Feli et al. [49] present an analytical model for low-velocity impact on CNT-reinforced plates. Vinyas [50] utilized the finite element method to analyze the vibrations of magneto-electro-elastic plates reinforced with carbon nanotubes (CNTs). Shen et al. [51] conducted an assessment of the nonlinear response of plates reinforced with carbon nanotubes (CNTs) when subjected to blast loads. Ensari et al. [52] conducted a study on the thermal buckling analysis of plates reinforced with FG-CNT, while another study by the same authors [53] focused on the vibration response of thick plates reinforced with CNTs. Sharma et al. investigated FG CNT-reinforced plates for buckling and free vibration [54]. Torabi et al. [55] employed the TSDT method to examine the thermal buckling behavior of composite plates reinforced with carbon nanotubes (CNTs). Zhou and Song [56] investigated the nonlinear bending behavior of composite plates reinforced with carbon nanotubes (CNTs) using the element-free Galerkin technique. The thermal and vibrational properties of plates reinforced with carbon nanotubes (CNTs) exhibiting a negative Poisson's ratio were investigated by Yang et al. [53]. Nguyen et al. [54] have employed the First-order Shear Deformation Theory (FSDT) to develop a model for analyzing the vibration response of 2D-FGM beams subjected to a moving load. The dynamic response of various beams under moving charges and loads has been investigated in previous studies [57–64]. Shi [65] employed iso-geometric analysis (IGA) to investigate the static bending, free vibration, and buckling characteristics of functionally graded carbon nanotube-reinforced composite plates. Other studies on the FGM-CNT material are also discussed in references [66, 67].

The movement of loads is a significant topic in various fields, including microelectromechanical systems (MEMS) and space applications. Furthermore, there is a lack of research on the dynamics of composite beams reinforced with FG-CNTs under the influence of moving loads in existing literature. This study focuses on the potential advanced applications of the moving load. It begins by developing a dynamic model for reinforced composite beams, specifically the uniform UD-CNT, X type (FGX-CNT), and type (FG-CNT) beams. The model incorporates a novel TSDT approach. The calculation involves determining the interaction between the moving load and the FG-CNT beams by considering the kinetic energy of the load's mass and the vibrating beam's kinetic and potential energies. This study extensively investigated the impact of carbon nanotube distribution across the thickness of a beam and the velocity of a moving charge on the dynamics of carbon nanotube-reinforced composite beams. The study's findings will aid in precisely designing nano-sensors capable of carrying live loads. Furthermore, it is believed that the findings of this study will have practical implications for the aerospace industry, particularly in the areas of advanced transfer applications in both macro and micro-dimensions.

Effective Properties of FG-CNT Beams Under a Moving Charge

Figure 1(a) depicts a moving charge and a composite beam with dimensions L, b, and h. In the context of the given information, the symbol L denotes the length of the beam, b represents its width, h signifies its height, and A denotes its cross-sectional area. Figure 1(b) illustrates three types of aligned carbon nanotube (CNT) reinforced beams: uniformly distributed CNT beams (UD-CNT), functionally graded CNT beams type X (FGX-CNT), and functionally graded CNT beams type (FG-CNT). The FGX-CNT beams have concentrated CNT in both the upper and lower regions, while the FG-CNT beams have densified CNT in the lower region. The reinforcement of carbon nanotubes (CNTs) is aligned along the longitudinal direction, specifically the x-axis. Assuming uniform beam diameters, total weight (mTCNT), and volume percentage (VTCNT) of carbon nanotubes (CNTs), the distribution of CNTs in the X kinds follows a power law. The range [1, 55] represents the distribution of carbon nanotubes (CNTs) in the thickness direction of FG-CNT.

$$\mu(z) = \left(\frac{h-2z}{2h}\right)^k, \left(-\frac{h}{2} \le z \le \frac{h}{2}\right). \tag{1}$$

So, the volume fraction of CNTs that corresponds to that is described by:

$$V_{CNT}(z) = (k+1)\left(\frac{h-2z}{2h}\right)^k V_{TCNT}, \left(-\frac{h}{2} \le z \le \frac{h}{2}\right). \tag{2}$$

The distribution and volume fraction of CNTs for X-type FGX-CNT is [10]:

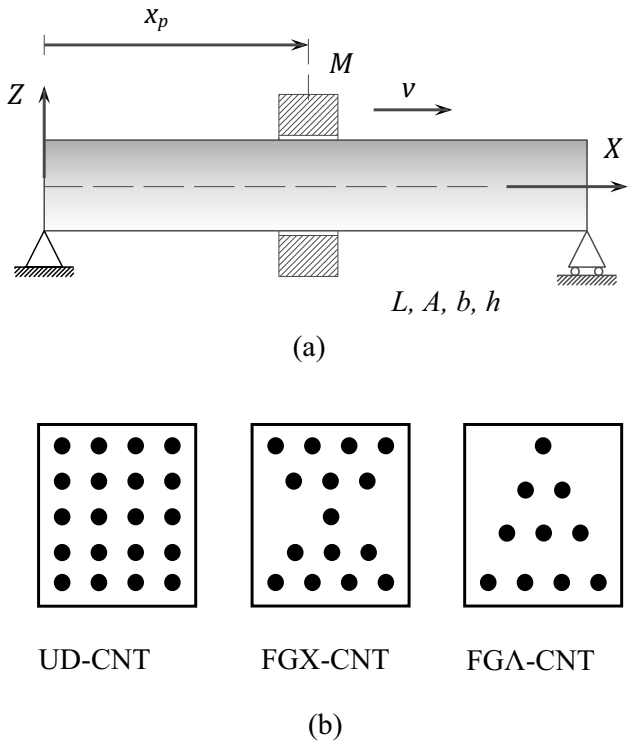

Fig. 1 **a** FG-CNT reinforced beam subjected to a moving charge M, **b** cross section of several beam types, UD-CNT, FGX-CNT, and FGΛ-CNT

$$\mu(z) = \begin{cases} \left(\frac{2z}{h}\right)^k \left(0 \le z \le \frac{h}{2}\right), \\ \left(-\frac{2z}{h}\right)^k \left(-\frac{h}{2} \le z \le 0\right). \end{cases} \tag{3}$$

$$V_{CNT}(z) = \begin{cases} (k+1)\left(\frac{2z}{h}\right)^k V_{TCNT} \left(0 \le z \le \frac{h}{2}\right), \\ (k+1)\left(-\frac{2z}{h}\right)^k V_{TCNT} \left(-\frac{h}{2} \le z \le 0\right). \end{cases} \tag{4}$$

In the case of uniform (UD-CNT) beams, the distribution is:

$$V_{CNT}(z) = V_{TCNT}, \left(-\frac{h}{2} \le z \le \frac{h}{2}\right). \tag{5}$$

The outcomes of MD simulations and mixing rule [3, 4] are used to evaluate the practical material attributes. Consequently, the properties' formulations are [1].

$$E_{22}(z) = \frac{\eta_2}{\frac{V_{CNT}(z)}{E_{22}^{cnt}} + \frac{V_m(z)}{E^m}} \tag{6a}$$

$$E_{11}(z) = \eta_1 V_{CNT}(z) E_{11}^{cnt} + V_m(z) E^m, \tag{6b}$$

$$G_{12}(z) = \frac{\eta_3}{\frac{V_{CNT}(z)}{G_{12}^{cnt}} + \frac{V_m(z)}{G^m}}, \tag{6c}$$

$$\upsilon_{21}(z) = \frac{\upsilon_{12}(z)}{E_{11}(z)} E_{22}(z), , \tag{6d}$$

$$\upsilon_{12}(z) = V_{CNT}(z)\upsilon_{12}^{cnt} + V_m(z)\upsilon^m \tag{6e}$$

$$\rho(z) = V_{CNT}(z)\rho^{cnt} + V_m(z)\rho^m, \tag{6f}$$

$$V_m(z) = 1 - V_{CNT}(z). \tag{6g}$$

Here,E^m,G^m,E_{11}^{cnt},E_{22}^{cnt}, G_{12}^{cnt} are Young's modulus and shear modulus of matrix and CNT, $\eta_i, (i = 1, 2and3)$ are efficiency parameters of CNT/matrix; υ^m and υ_{12}^{cnt} are Poisson's ratios of matrix and CNT, and ρ^m and ρ^{cnt} are mass densities of matrix and CNT, respectively. E(z) and G(z) are effectively provided by [10] as;

$$E(z) = \frac{E_{11}(z)}{1 - \upsilon_{12}(z)\upsilon_{21}(z)},$$

$$G(z) = G_{12}(z) \tag{7}$$

Mathematical Formulation

The literature has different types of beam and plate theories for the shear deformation effect. In this study, we used a refined sinusoidal third-order shear deformation model (SSDT) [68]. The displacement field is in the form:

$$\begin{aligned} cu_1(x,z,t) &= u_0(x,t) - z\frac{\partial w_0}{\partial x} + f(z)\phi(x,t), \\ u_2(x,z,t) &= 0, \\ u_3(x,z,t) &= w_0(x,t) \end{aligned} \tag{8}$$

Here, u_1, u_2, and u_3 denote the displacements in x, y, and z axes, respectively, and $u(x,t)$ and $w(x,t)$ represent the mid-plane displacements in the axial and transverse directions, and $\phi(x,t)$ is the rotation of the cross-section. Thus, strain as [69]:

$$c\varepsilon_{xx} = \varepsilon_{xx}^0 - z\varepsilon_{xx}^1 + f(z)\varepsilon_{xx}^2,$$
$$\gamma_{xz} = \frac{df(z)}{dz} \tag{9}$$
$$f(z) = z - \frac{h}{\pi} sin\left(\frac{\pi z}{h}\right).$$

With

$$\varepsilon_{xx}^0 = \frac{\partial u}{\partial x} - \frac{1}{2}\left(\frac{\partial w}{\partial x}\right)^2, \varepsilon_{xx}^1 = \frac{\partial^2 w}{\partial x^2}, \varepsilon_{xx}^2 = \frac{\partial \phi_x}{\partial x} \tag{10}$$

Constitutive relationships can be expressed as follows:

$$\begin{Bmatrix} \sigma_{xx} \\ \tau_{xz} \end{Bmatrix} = \begin{bmatrix} Q_{11} & 0 \\ 0 & Q_{66} \end{bmatrix} \begin{Bmatrix} \varepsilon_{xx} \\ \gamma_{xz} \end{Bmatrix} \tag{11}$$

The stiffnesses are

$$Q_{11} = \frac{E(z)}{1-\upsilon^2}, Q_{66} = \frac{E(z)}{2(1+\upsilon)} \tag{12}$$

Based on the NGST, the total normal and shear stress are derived as [70]:

$$\sigma_{xx} = \left[1 - l_m^2 \nabla^2\right] E(z)\varepsilon_{xx},$$
$$[1 - (ea)^2\nabla^2]\tau_{xx} = \left[1 - l_m^2\nabla^2\right] G(z)\gamma_{xx}, \tag{13}$$

where ε_{xx} and γ_{xz} are the axial and shear strains. Ignoring the effects of thermal expansion in other directions except for the axial direction, the first part of the Eq. (13) is modified as follows:

$$\sigma_{xx}^t - (ea)^2 \frac{\partial^2 \sigma_{xx}^t}{\partial x^2} = \left[\varepsilon_{xx} - l_m^2 \frac{\partial^2 \varepsilon_{xx}}{\partial x^2}\right] E(z)$$
$$\sigma_{xz}^t - (ea)^2 \frac{\partial^2 \tau_{xz}^t}{\partial x^2} = \left[\gamma_{xz} - l_m^2 \frac{\partial^2 \gamma_{xz}}{\partial x^2}\right] G(z) \tag{14}$$

The force and moment resultants can be expressed as

$$\begin{Bmatrix} N_{xx} \\ M_{xx} \\ P_{xx} \end{Bmatrix} = \int_{-h/2}^{h/2} \begin{Bmatrix} 1 \\ z \\ f(z) \end{Bmatrix} \sigma_{xx} dz,$$
$$Q_{xz} = \int_{-h/2}^{h/2} \frac{df(z)}{dz} \tau_{xz} dz. \tag{15}$$

Using the above equations, the force and moment resultants in the function of the strains are given as

$$\begin{Bmatrix} N_{xx} \\ M_{xx} \\ P_{xx} \end{Bmatrix} = \begin{bmatrix} A_{11} & B_{11} & C_{11} \\ B_{11} & D_{11} & F_{11} \\ C_{11} & F_{11} & H_{11} \end{bmatrix} \begin{Bmatrix} \varepsilon_{xx}^0 \\ \varepsilon_{xx}^1 \\ \varepsilon_{xx}^2 \end{Bmatrix},$$
$$Q_{xz} = J_{66}\gamma_{xz} \tag{16}$$

The stiffness coefficients are given as follows:

$$(A_{11}, B_{11}, C_{11}, D_{11}, F_{11}, H_{11}) = b\int_{-\frac{h}{2}}^{\frac{h}{2}} (1, z, z^2, f(z), zf(z), f(z)^2) Q_{11} dz.$$
$$J_{66} = b\int_{-h/2}^{h/2} \left(\frac{df(z)}{dz}\right)^2 Q_{66} dz \tag{17}$$

The principle of Hamilton is applied here to formulate the equations of motion of the CNTRC beams [71]:

$$\int_{t1}^{t2} (\delta T - \delta U + \delta V) dt = 0 \tag{18}$$

U, T, and V are the total deformation energy, the kinetic energy, and the external potential energy, respectively. The total deformation energy of the current problem can be written as

$$U = \frac{1}{2}\int_V (\sigma_{xx}\varepsilon_{xx} + \tau_{xz}\gamma_{xz}) dV \tag{19}$$

$$= \frac{1}{2}\int_0^L \left(N_{xx}\varepsilon_{xx}^0 + M_{xx}\varepsilon_{xx}^1 + P_{xx}\varepsilon_{xx}^2 + Q_{xz}\gamma_{xz}\right) dx \tag{20}$$

The variation of the kinetic energy at any moment is stated as

$$T = \frac{1}{2}\int_0^l \int_A \rho(z)\left[(\dot{u}^2 + \dot{w}^2)\right] dA dx \tag{21}$$

In addition, the variation of external potential energy generated by the applied load can be expressed as:

$$V = \frac{1}{2}\int_0^l \left[q(x,t)\delta w + P\frac{\partial w}{\partial x}\frac{\partial \delta w}{dx}\right] dx \tag{22}$$

where $q\ (x, t)$ and P is the transverse and axial loads, respectively. This study demonstrates the inclusion of the axial load P within the general formula. Furthermore, it is observed that no axial load is applied in this study as a result of the moving mass. By substituting Eqs. (20), (21), and (22) into Eq. (18) and after the integration, setting each coefficient of $\delta u_0, \delta w_0$ and $\delta \phi_x$ to zero, the equations of motion for the used sinusoidal higher-order shear deformation beam theory are:

$$\delta u_0 : \frac{\partial N_{xx}}{\partial x} = I_0\frac{\partial^2 u_0}{\partial t^2} - I_1\frac{\partial^3 w_0}{\partial x \partial t^2} + I_3\frac{\partial^2 \phi_x}{\partial t^2},$$
$$\delta w_0 : \frac{\partial^2 M}{\partial x^2} = P\frac{\partial^2 w_0}{\partial x^2} + I_0\frac{\partial^2 w_0}{\partial t^2} + I_1\frac{\partial^3 u_0}{\partial x \partial t^2} - I_2\frac{\partial^4 w_0}{\partial x^2 \partial t^2} + I_4\frac{\partial^3 \phi_x}{\partial x \partial t^2},$$
$$\delta \phi_x : \frac{\partial P}{\partial x} - Q_{xz} = I_3\frac{\partial^2 u_0}{\partial t^2} - I_4\frac{\partial^3 w_0}{\partial x \partial t^2} + I_5\frac{\partial^2 \phi_x}{\partial t^2} \tag{23}$$

With the inertia coefficients:

$$(I_0, I_1, I_2, I_3, I_4, I_5) = b\int_{-h/2}^{h/2} \rho(z)(1, z, z^2, f(z), zf(z), f(z)^2) dz \tag{24}$$

The equations of motion of nonlocal strain gradient nanoplate can be governed.

$$
\begin{aligned}
&c\left(1-l_m^2\frac{\partial^2}{\partial x^2}\right)\left(A_{11}\frac{\partial^2 u}{\partial x^2}-B_{11}\frac{\partial^3 w}{\partial x^3}+C_{11}\frac{\partial^2 \phi}{\partial x^2}\right)\\
&+\left(1-(ea)^2\frac{\partial^2}{\partial x^2}\right)\left(-I_0\frac{\partial^2 u_0}{\partial t^2}+I_1\frac{\partial^3 w_0}{\partial x\partial t^2}-I_3\frac{\partial^2 \phi_x}{\partial t^2}\right)=0,\\
&\left(1-l_m^2\frac{\partial^2}{\partial x^2}\right)\left(B_{11}\frac{\partial^3 u}{\partial x^3}-D_{11}\frac{\partial^4 w}{\partial x^4}+F_{11}\frac{\partial^3 \phi}{\partial x^3}\right)+\left(1-(ea)^2\frac{\partial^2}{\partial x^2}\right)\\
&\left(-P\frac{\partial^2 w_0}{\partial x^2}-I_0\frac{\partial^2 w_0}{\partial t^2}-I_1\frac{\partial^3 u_0}{\partial x\partial t^2}+I_2\frac{\partial^4 w_0}{\partial x^2\partial t^2}-I_4\frac{\partial^3 \phi_x}{\partial x\partial t^2}\right)=0,\\
&\left(1-l_m^2\frac{\partial^2}{\partial x^2}\right)\left(C_{11}\frac{\partial^2 u}{\partial x^2}-F_{11}\frac{\partial^3 w}{\partial x^3}+H_{11}\frac{\partial^2 \phi}{\partial x^2}+J_{66}\phi\right)\\
&+\left(1-(ea)^2\frac{\partial^2}{\partial x^2}\right)\left(-I_3\frac{\partial^2 u_0}{\partial t^2}+I_4\frac{\partial^3 w_0}{\partial x\partial t^2}-I_5\frac{\partial^2 \phi_x}{\partial t^2}\right)=0
\end{aligned}
\tag{25}
$$

Analytical Solution

Navier's approach will be used to define the vibration frequencies and displacements for the simply supported boundary conditions. For the classical boundary conditions in Eq. (25) (at $x = 0$ and $x = L$)

$$N_{xx} = 0, w = 0, M = 0, \tag{26}$$

And for non-classical boundary conditions (at $x = 0$ and $x = L$)

$$\frac{\partial u}{\partial x} = 0, Q_{xz}^h = 0, \frac{\partial \phi}{\partial x} = 0, \tag{27}$$

Assuming the vibration solution is periodic in time, the displacements are in the form:

$$
\begin{aligned}
u(x,t) &= \textstyle\sum_n U_n \cos\gamma x e^{i\omega_n t}\\
w(x,t) &= \textstyle\sum_n W_n \sin\gamma x e^{i\omega_n t}\\
\phi(x,t) &= \textstyle\sum_n \Phi_n \cos\gamma x e^{i\omega_n t}
\end{aligned}
$$

$$\gamma = \left(\frac{n\pi}{L}\right), \tag{28}$$

where $i = \sqrt{-1}$, and ω_n is the natural vibration frequencies. For any U_n, W_n and Φ_n, the series solution (28) satisfies the classical and non-classical boundary conditions in (26) and (27). The following eigenvalue equation is derived by substituting Eq. (28) into Eq. (25).

$$\left(\mathbf{K} - P\mathbf{K_G} - \omega_n^2\mathbf{M}\right)\mathbf{d} = 0, \tag{29}$$

Here, $\mathbf{d} = \left\{ U_n \;\; W_n \;\; \Phi_n \right\}^T$ are the unknowns to be determined, $\mathbf{K}$, $\mathbf{K_G}$ and $\mathbf{M}$ are stiffness, geometric stiffness, and mass matrices, respectively. Moreover, the coefficients of them are described as follows:

$$\mathbf{K}_{11} = -A_{11}c_2\gamma^2, \mathbf{K}_{13} = -B_{11}c_2\gamma^3, \mathbf{K}_{13} = C_{11}c_2\gamma^2$$

$$\mathbf{K}_{21} = B_{11}\gamma^3 c_2, \mathbf{K}_{22} = -D_{11}\gamma^4 c_2, \mathbf{K}_{23} = -F_{11}\gamma^3 c_2,$$

$$\mathbf{K}_{31} = \mathbf{K}_{13}, \mathbf{K}_{32} = \mathbf{K}_{23}$$

$$\mathbf{K}_{33} = \left(H_{11}\gamma^2 + J_{66}\right)c_2, \mathbf{K}_{\mathrm{G}22} = -\gamma^2 c_1$$

$$\mathbf{M}_{11} = I_0 c_1, \mathbf{M}_{12} = -I_1\gamma c_1, \mathbf{M}_{13} = I_3 c_1,$$

$$\mathbf{M}_{21} = \mathbf{M}_{12}, \mathbf{M}_{22} = (I_0 + I_2\gamma^2)c_1, \mathbf{M}_{23} = -I_4\gamma c_1$$

$$\mathbf{M}_{31} = \mathbf{M}_{13}, \mathbf{M}_{32} = \mathbf{M}_{23}, \mathbf{M}_{33} = I_5 c_1$$

$$c_1 = 1 + (ea)^2\gamma^2, c_2 = 1 + l_m^2\gamma^2, \tag{30}$$

For the forced vibration response of the FG Timoshenko nanobeam, substituting Eq. (28) into (25), one can derive the following equation:

$$\mathbf{M}\ddot{\mathbf{d}} + (\mathbf{K} - P\mathbf{K_G})\mathbf{d} = \mathbf{F}, \tag{31}$$

where $\mathbf{F}$ is the external force vector, and it can be defined according to the type of the transverse load $q(x)$ as given below [71]:

$$\mathbf{F} = \begin{Bmatrix} 0 \\ Q_n c_1 \\ 0 \end{Bmatrix}, \tag{32}$$

The external load can be expanded in the Fourier series, and the term Q_n is defined as follows:

$$q(x) = \sum_n Q_n \sin\frac{n\pi x}{L}, \tag{33a}$$

$$Q_n = \frac{2}{L}\int_0^L q(x)\sin\frac{n\pi x}{L}dx, \tag{33b}$$

For point load at x_p, the external load is defined as $q(x) = F\delta(x - x_p)$ and Q_n is derived as:

$$Q_n = \frac{2F}{L}\sin\frac{n\pi}{L}x_p, n = 1, 2, 3, \ldots$$

$$x_p = L/2; \overset{yields}{\rightarrow} Q_n = \frac{2F}{L}\sin\frac{n\pi}{2}, n = 1, 2, 3, \ldots, \tag{34a}$$

Table 1 Comparison of the frequency parameter (λ_1) between Al_2O_3 and Al for the simply supported FGM beam

Power-law exponent k	References	Fundamental frequency, λ_1		
		$L/h=10$	$L/h=30$	$L/h=100$
0	Present	2.8027	2.8434	2.8483
	From [72]	2.7970	2.8430	2.8480
	From [73]	2.8026	2.8438	2.8486
	From [74]	2.8027	2.8458	2.8488
0.3	Present	2.6992	2.7362	2.7414
	From [72]	2.6950	2.7370	2.7420
	From [73]	2.6992	2.7368	2.7412
	From [74]	2.6953	2.7361	2.7421

Table 2 Comparison of the maximum midspan reactions of FGM beams

Source	SUS304 (132 m/s)	$k=0.2$ (222 m/s)	$k=0.5$ (198 m/s)	$k=1$ (179 m/s)	$k=2$ (164 m/s)	$k=5$ (164 m/s)	Al_2O_3 (252 m/s)
Present	1.7318	1.0338	1.1432	1.2694	1.3361	1.6316	0.9327
[75]	1.7324	1.0344	1.1444	1.2503	1.3376	-	0.9328
[76]	1.7301	1.0333	1.1429	1.2486	1.3359	-	0.9317

Table 3 CNT efficiency parameters [10]

CNT efficiency parameters	V_{TCNT}		
	0.12	0.17	0.28
η_1	0.137	0.142	0.141
η_2	1.022	1.626	1.585
η_3	0.715	1.138	1.109

For uniform load:

$$q(x) = q_0, Q_n = \frac{4q_0}{n\pi}, n = 1, 3, 5, \ldots \tag{34b}$$

Results

Numerical Verification

To check the accuracy of the proposed method, a FGM beam made of alumina and aluminum, studied by [72–74], is considered. As used in the literature, the fundamental non-dimensional frequency parameter λ_1 is described as follows:

$$\lambda_1 = \omega_1 L^2 \left(\int_{-h/2}^{h/2} \rho(z) dz \right)^{\frac{1}{2}} \left(h^2 \int_{-h/2}^{h/2} E(z) dz \right)^{\frac{-1}{2}} \tag{35}$$

For different power-law exponent k and slenderness ratios L/h, the analysis results are given in Table 1. As seen in Table 1, the present study's results and the literature's results are in good agreement.

Another FGM beam subjected to a moving load is analyzed to compare the forced response results. The constituents of the beam material are alumina and stainless steel (SUS 304), and the properties of the beam are the same as those given by [75, 76]. In Table 2, the results are very close to those in the literature.

TFor more comparison, the following material properties [10, 77] are used: $E^m = 2.5GPa, \upsilon^m = 0.3, E_{11}^{cnt} = 5646.6GPa$, $E_{22}^{cnt} = 7080GPa$, $G_{12}^{cnt} = 1944.5GPa$, $\upsilon_{12}^{cnt} = 0.175$, $\rho^m = 1190kg/m^3$, $\rho^{cnt} = 2100kg/m^3$, $h = 0.1m$, with the efficiency parameters of CNT in Table 3 [10]. The dimensionless frequency parameter is defined as [10].

Table 4 Presentation of the frequency values λ_1 of FG-CNT beams, $V_{TCNT} = 0.12, (L/h = 10)$.

Boundary cond	FGΛ-CNT		FGX-CNT		UD-CNT	
	Present	References [10]	Present	References [10]	Present	References\ [8]
P-P	1.2291	1.2296	1.3856	1.3852	1.2571	1.2576
C-P	1.3942	1.3944	1.5387	1.5385	1.4552	1.4556
C–C	1.6059	1.6063	1.7232	1.7230	1.6673	1.6678

Table 5 The first three frequency parameters $\lambda_1, \lambda_2, \lambda_3$, for different FG-CNT beams with $V_{TCNT} = 0.28, (L/h = 15)$, (P-P) boundary conditions

CNT distribution	Mode	Present study	Reference [10]	Reference [8]
FGΛ-CNT	1	1.4015	1.3975	1.4027
	2	3.8475	3.8370	3.8639
	3	6.7325	6.6976	6.7618
FGX-CNT	1	1.6445	1.6409	1.6493
	2	4.4465	4.4333	4.4752
	3	7.3023	7.2258	7.3068
UD-CNT	1	1.4378	1.4348	1.4401
	2	4.1254	4.1050	4.1362
	3	6.9015	6.8595	6.9245

$$\lambda_i = \omega_i L \sqrt{\rho^m \left[1 - (\upsilon^m)^2\right] / E^m} \tag{36}$$

Three boundary conditions are examined in the analysis: Clamped–Clamped (C–C), Clamped–Pinned (C-P), and Pinned–Pinned (P-P). Table 4 compares the fundamental frequency parameter λ_1 for a total CNT volume percentage of 0.12 and a slenderness ratio of L/h = 10. After numerous convergence investigations, the results are in excellent agreement with the literature, particularly those of [10], which accounts for N = 15 terms in the Ritz technique.

Table 5 displays the first three frequency parameters $\lambda_1, \lambda_2, \lambda_3$ for various FG-CNT beams with a total volume percentage of CNT V TCNT = 0.28, slenderness ratio L/h = 15, and (P-P) boundary conditions to compare the new formulation with the literature. The results of the current study are roughly equivalent to those of the Ritz technique with $N = 15$ terms [10] and the generalized differential quadrature method (GDQM) [8] with $N = 9$ grid points.

Depending on the CNT volume fractions, slenderness ratios, and distribution types, the fundamental frequency parameter λ_1 is calculated. Table 6 shows the comparisons of fundamental frequencies $\lambda_1 = \omega_1 L^2 \sqrt{\rho_m/(E_m h^2)}$ of different nanobeams for V_{TCNT} and L/h. As seen from Table 6, for the same slenderness ratio and CNT volume fraction, the fundamental frequency of the FGX type is more significant than FGΛ, and the fundamental frequencies in the UD type are the lowest. In the case of a FGX distribution, it can be observed that carbon nanotubes tend to be more concentrated in the outer regions of the beam. The functional gradation of the material results in increased inertia and bending resistance. Due to this reason, given that the natural frequencies within the FGX distribution exhibit higher values in comparison to the other distributions, it is observed that the FGX distribution resonates, thereby yielding maximum response, at elevated load speeds relative to the remaining distributions.

Table 7 Material properties [74]

Properties	Alumina (Al_2O_3)	Stainless steel (SUS304)
E	390 GPa	210 GPa
ρ	3960 GPa	8166 GPa
υ	0.3	0.3177

Table 8 Comparison of maximum midpoint displacements for isotropic solid beam under a moving charge

Source	$V = 132$ m/s	$V = 252$ m/s
Present	1.7309	0.9321
Ref. [74]	1.7316	0.9326
Ref. [75]	1.7324	0.9328
Ref. [76]	1.7301	0.9317

To enhance the verification of the research, we include an analysis of beam. This beam has been extensively studied in existing literature and is characterised by the materials Al $_2O_3$ and SUS 304. The specific properties of the beam are provided in Table 7. Table 8 presents the findings derived from the conducted study, along with the corresponding values cited in the literature [74–76]. Table 4 presents the findings of the current study, which demonstrate a high degree of similarity to the results reported in previous scholarly works, particularly those documented in reference [75].

Case Study

Using the same material properties given above for interaction with the moving load, numerous analyses have been made considering the velocity of the load. The slenderness ratio is chosen as $L/h = 10$, and the thickness and width of

Table 6 Comparisons of fundamental frequencies $\lambda_1 = \omega_1 L^2 \sqrt{\rho_m/(E_m h^2)}$ of different nanobeams for V_{TCNT} and L/h,

	UD			FGΛ			FGX		
V_{TCNT}	L/h = 5	L/h = 15	L/h = 25	L/h = 5	L/h = 15	L/h = 25	L/h = 5	L/h = 15	L/h = 25
0.12	6.7032	13.8745	15.6102	6.9952	13.5905	15.4143	7.2033	15.3266	18.0963
0.17	8.6415	16.8298	18.6968	8.8390	16.5389	18.5005	9.1412	18.8007	21.8404
0.28	9.3455	19.4747	22.3750	9.4854	19.1949	22.1377	9.7305	21.4979	25.8978

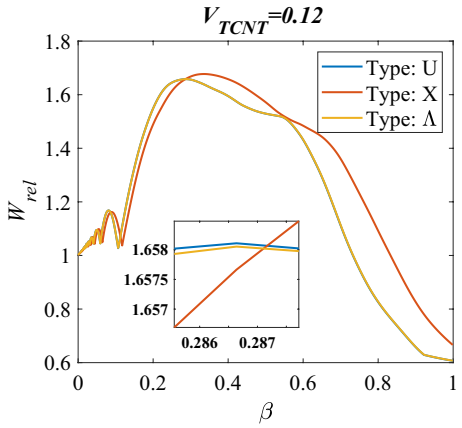

Fig. 2 The comparisons of normalized maximum mid-point displacements of different FG-CNT reinforced beams for $V_{TCNT} = 0.12$. The zoomed window: the curves about β = 0.286 where the DAFs of UD-CNT and FGΛ-CNT are nearly at the maxima

the beams are $h = b = 1$ m. For the power-law exponent, $k = 1$ is used unless otherwise stated. A parametric moving load velocity is applied between $\beta = 0$ and 1, where $\beta = v/v_{cr}$, $v_{cr} = \omega/\omega_1$, ω: the loading frequency of the moving load with $\omega = \pi v/L$, [78] and ω_1 is the fundamental natural frequency of UD-CNT beam. The dynamic interaction analysis is carried out by Newmark numerical integration procedure with 500-time steps. The mass of the load is $M = 100$ kg for all analyses, and dynamic amplification factors (DAFs) are defined as the ratio of the maximum midspan displacement to the static displacement where the load is in the midspan of the beams. The DAFs are normalized for their static displacement for each type of composite beam. The normalized amplitude of the DAFs, W_{rel} is defined as:

$$W_{rel} = w_{max}(L/2, t)/w_s \tag{37}$$

where w_s is the static mid-span displacement, with:

$$w_s = \frac{MgL^3}{48EI} \tag{38}$$

Figure 2 presents the normalized dynamic displacements of the midpoints of the UD-CNT, FGX-CNT, and FGΛ-CNT beams according to the dimensionless velocity (speed parameter) of the moving load for the total volume fraction of CNTs $V_{TCNT} = 0.12$. For this value, the dynamic characteristics of the UD-CNT and FGΛ-CNT beams appear to be very close to each other, and when compared to each other, the uniform UD-CNT is slightly weaker in stiffness than FGΛ-CNT. While the maximum displacement values of these two occur at $\beta = 0.286$ of the speed parameter, the maximum displacement of the FGX-CNT beam occurs at $\beta = 0.34$. This means that the FGX-CNT beam is weaker than the others regarding dynamic stiffness but better than the others regarding resonance performance. One of the reasons for this feature of the FGX-CNT beam is that the effective mass is distributed close to the lower and upper planes of the beam, away from the neutral beam axis, and similar behaviors are seen in Figs. 3a and b. The results of the analysis are presented for $V_{TCNT} = 0.17$ in Fig. 3a and $V_{TCNT} = 0.28$ in Fig. 3b. Also, the maximum response value for Type X is observed to be 1.68, with this maximum occurring at $\beta = 0.5$. In the case of type U, the maximum response is observed at β values of 0.35 and 1.66. Similarly, for type Λ, the maximum response is observed at β values of 0.34 and 1.657. This implies that the natural frequency of the beam, characterized by a material distribution that elicits a greater response at higher velocities compared to alternative distribution types, exhibits a higher magnitude relative to the remaining distributions. An increase in frequency corresponds to an increase in strength. Hence, it has been demonstrated that the FGX distribution exhibits a greater frequency in comparison to the remaining distributions. As the total ratio of CNTs in the beam increases, the speed parameters at which maximum displacements occur in all beam types also increase. This means that the CNT addition

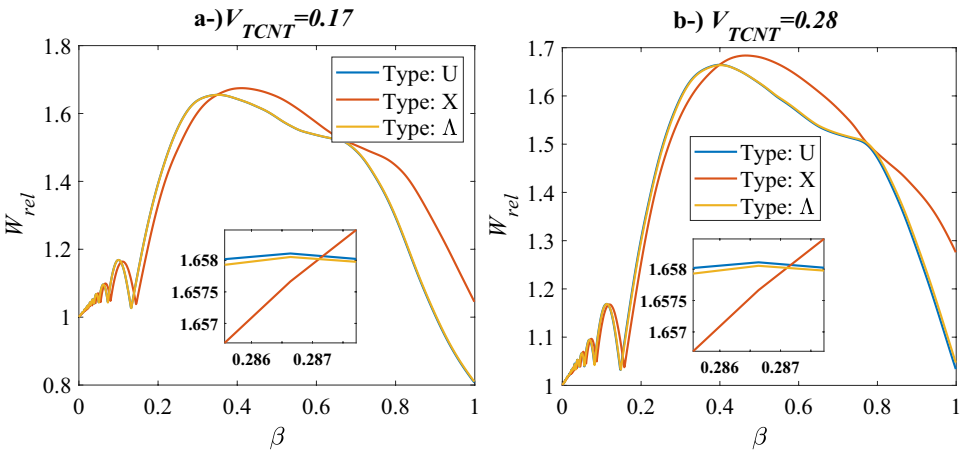

Fig. 3 The presentation of normalized mid-point deflections of different FG-CNT reinforced beams for **a** $V_{TCNT} = 0.17$, **b** $V_{TCNT} = 0.28$. The zoomed windows: the curves about $\beta = 0.286$ where the DAFs of UD-CNT and FGΛ-CNT are nearly at the maxima

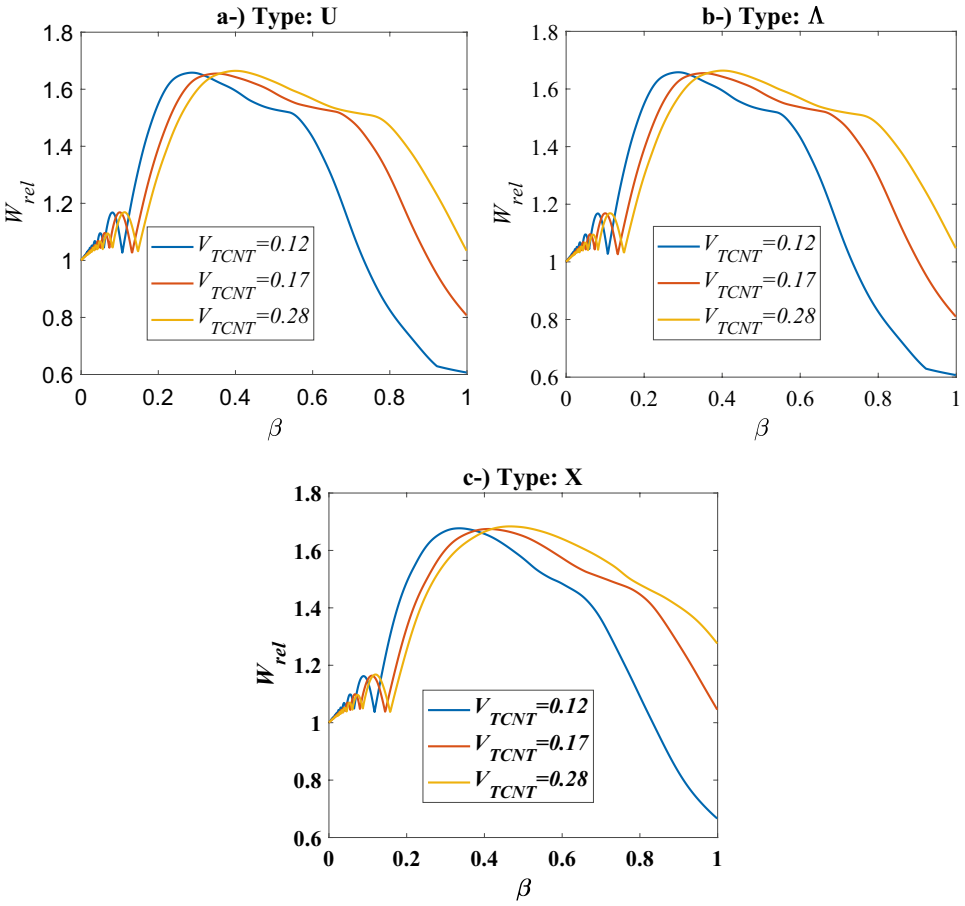

Fig. 4 The presentation of normalized mid-point deflections of CNT-reinforced beams for different total volume fractions $V_{TCNT} = 0.12, 0.17 and 0.28$. **a** UD-CNT. **b** FGΛ-CNT. **c** FGX-CNT

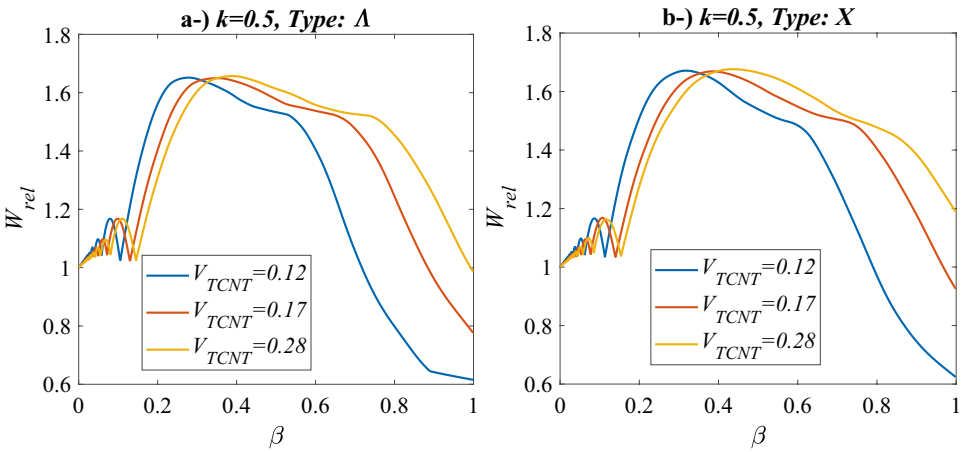

Fig. 5 The comparisons of normalized maximum mid-point displacements of CNT reinforced beams for different total volume fractions $V_{TCNT} = 0.12, 0.17 and 0.28$, and power-law exponent $k = 0.5$. **a** FGΛ -CNT. **b** FGX-CNT

raises the resonant frequency of the beam, and the possible resonance will occur at higher speeds of the moving load. From this, we can conclude that CNT reinforcement will provide a better dynamic behavior than beams that are not reinforced. This result may be helpful for beams to be used in high-speed applications of moving charge problems.

For V_{TCNT}=0.12, 0.17, and 0.28, Fig. 4a, b and c show the dynamic behaviors of UD-CNT, FGX-CNT and FGΛ-CNT reinforced beams, respectively. Similar to the results of the previous analysis, the FGX-CNT reinforced beams have the best resonance behavior, showing maximum displacement at higher mass speeds when compared to the other beam types. The UD-CNT reinforced beam looks slightly better than the FGΛ-CNT reinforced beam in terms of mass velocity at which it undergoes resonance. The increase in the total volume fraction of CNTs in all three beam types causes maximum displacements at higher mass velocities. That is,

the addition of CNT improves the dynamic behavior of the beam, which would be advantageous for applications where high strength, lightness, and better resonance behavior are desired.

For the total volume fractions V_{TCNT} = 0.12, 0.17, and 0.28 values with power-law index $k=0.5$, Fig. 5a and Fig. 5b show the dynamic response of FGA-CNT and FGX-CNT reinforced beams, respectively. It is understood from the graphs that the value of $k=0.5$ decreases the velocities at which the maximums occur when compared to the results of $k=1$. In Fig. 5a, it was observed that the maximum displacement occurred at $\beta=0.279$ for V_{TCNT} = 0.12, whereas for the same V_{TCNT} The maximum displacement occurred at $\beta=0.287$, as given in Fig. 1. Similar behavior is also valid for FGX-CNT reinforced beams in Fig. 5b. In Fig. 5b, the maximum displacement occurs at $\beta=0.32$ for V_{TCNT}= 0.12, while the maximum displacement occurs at $\beta=0.34$ for the same V_{TCNT} in Fig. 1. For the other V_{TCNT}= 0.17 and 0.28, decreasing the value of k decreases the speed parameter at which the maximum displacements occur.

To better understand the dynamic behavior of FG-CNT beams, it is necessary to look at the time-dependent dynamic response of FG-CNT beams under the moving load. As previously mentioned, the ratio of the fundamental frequency to the excitation frequency [78] ($\omega = \pi L/v$) of the load is very important and it is obvious that the vibration amplitudes of the beams increase as this ratio approaches 1. As is known, the vibration mode shape of the fundamental frequency of a simply supported beam is in the form of a half sine wave. The beam makes maximum dynamic displacement when the excitation frequency of the load is a complete sine wave while the beam vibrates [79, 80]. This event is a kind of resonance event. However, after a while, the moving charge will leave the span of the beam, and the effect of the moving load will be transient. Hence, this resonance becomes temporary, and the vibration amplitude of the beam increases limitedly. As it is different from other vibrating forced systems, it is not exposed to much dynamic excitation that will cause an excessive increase in vibration amplitude.

For this reason, unlike other forced vibrating beam systems, the dynamic behavior of beams forced by moving load is specific depending on the excitation frequency of the moving load, hence the beam system's speed, mass, and flexibility properties. When this issue is understood sufficiently, one can better understand the dynamic behavior of beam systems under moving loads. For this reason, the dynamic responses

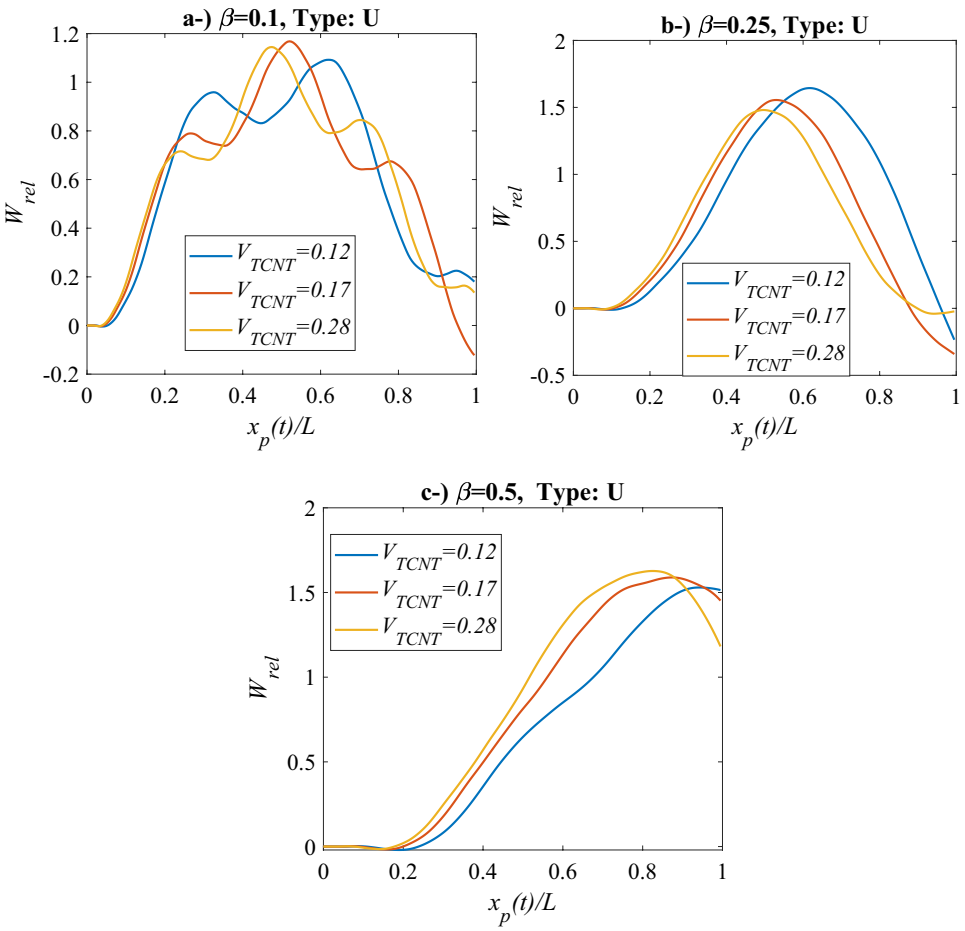

Fig. 6 The comparisons of normalized time histories of the mid-point displacements of UD-CNT reinforced beams for different total volume fractions V_{TCNT} = 0.12, 0.17*and*0.28, and dimensionless velocity β, **a** β = 0.1, **b** β = 0.25, **c** β = 0.5

of the considered beam types were investigated in detail, and the dynamic responses of UD-CNT reinforced beams at different speeds are presented in Figs. 6a, b, and c.

The dynamic responses of the UD-CNT reinforced beams based on the total CNT volume fractions are presented comparatively for the values $\beta = 0.1$ in Fig. 6a, $\beta = 0.25$ in Fig. 6b, and $\beta = 0.5$ in Fig. 6c. Looking at the dynamic behaviors of the UD-CNT reinforced beams with different total CNT volume fractions for the dimensionless load velocity $\beta = 0.1$ in Fig. 6a, it is seen that the dynamic displacements are different depending on the CNT amount. The number of full vibration waves seen in the response curves can be used to recognize the dynamic characteristics of the beam. Thus, in the curves given comparatively, the beam with the highest number of vibration waves behaves more rigidly than the others, and this beam is further away from the resonance zone for this speed. As the curves in the graphs show, the number of waves in UD-CNT beams with higher CNT addition is higher than in those with less CNT. The magnitude of the time-dependent dynamic response at a low speed also depends on the direction of the vibration waves so that it can be somewhat misleading. So, we cannot immediately say that the beam with the highest response is more flexible. However, in Fig. 6b, the vibration shape of the beams in all CNT ratios is almost like a half sine wave. Here, $\beta = 0.25$, and the vibration amplitudes are quite high since the beams are forced by an excitation load speed close to the maximum displacement zone of the beam. Here, the most flexible beam will have the highest vibration amplitude, and as seen from the curves, the beams with the lowest total CNT volume fraction at $V_{TCNT} = 0.12$ has the highest vibration amplitude, and the one with $V_{TCNT} = 0.28$ has the lowest vibration amplitude. Since the vibration wave numbers of the beams are very close and the vibration shapes are almost the same in this region, a relationship can be established between vibration amplitude and beam flexibility.

Depending on the time, the dynamic responses of the FGΛ-CNT reinforced beams are given in Figs. 7a, b, and c for $\beta = 0.1$, 0.25, and 0.5 values, respectively. Moreover, for the same values of β, in Figs. 8a, b, and c, the time-dependent dynamic responses of the FGX-CNT reinforced beams are given, respectively. In the time-dependent dynamic behavior of these beams, the speed of the load, the excitation frequency of this speed, and the distance of this frequency to the resonance zone are essential. Compared to each other, it is observed that FGX-CNT reinforced beams

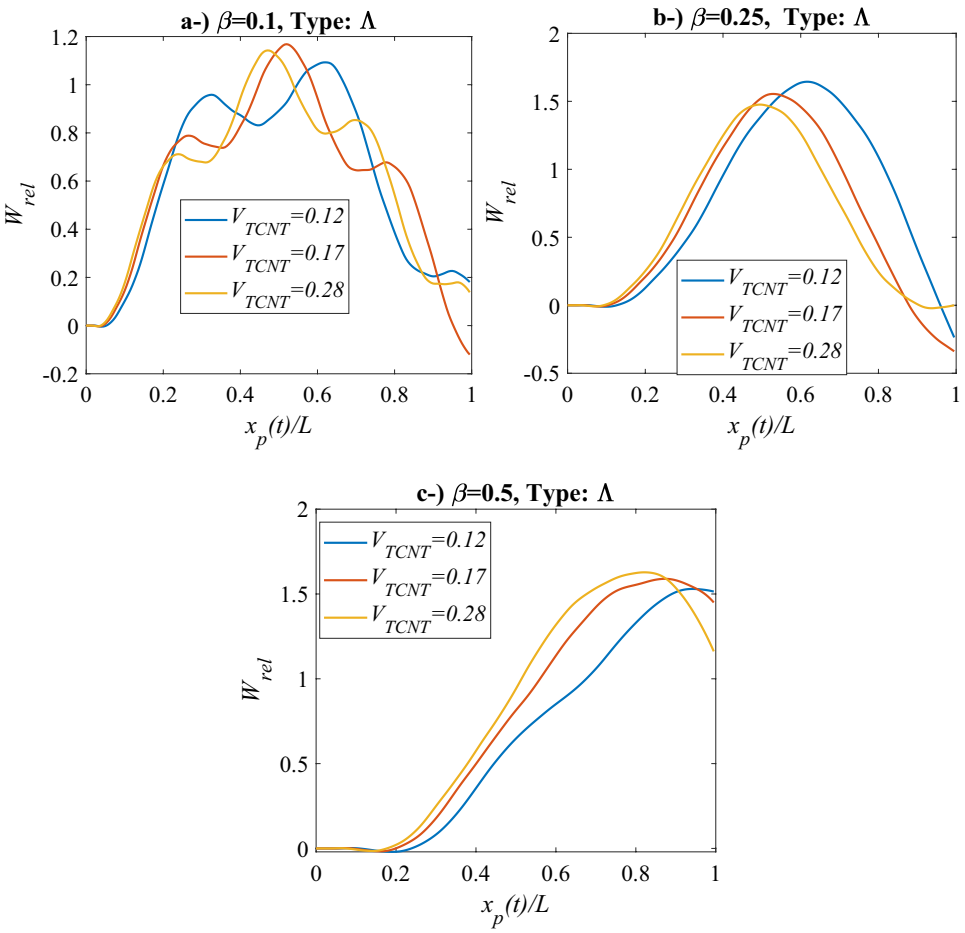

Fig. 7 The comparisons of normalized time histories of the mid-point displacements of FGΛ-CNT reinforced beams for different total volume fractions$V_{TCNT} = 0.12, 0.17 and 0.28$, and dimensionless velocity β. **a**$\beta = 0.1$, **b**$\beta = 0.25$, **c** $\beta = 0.5$

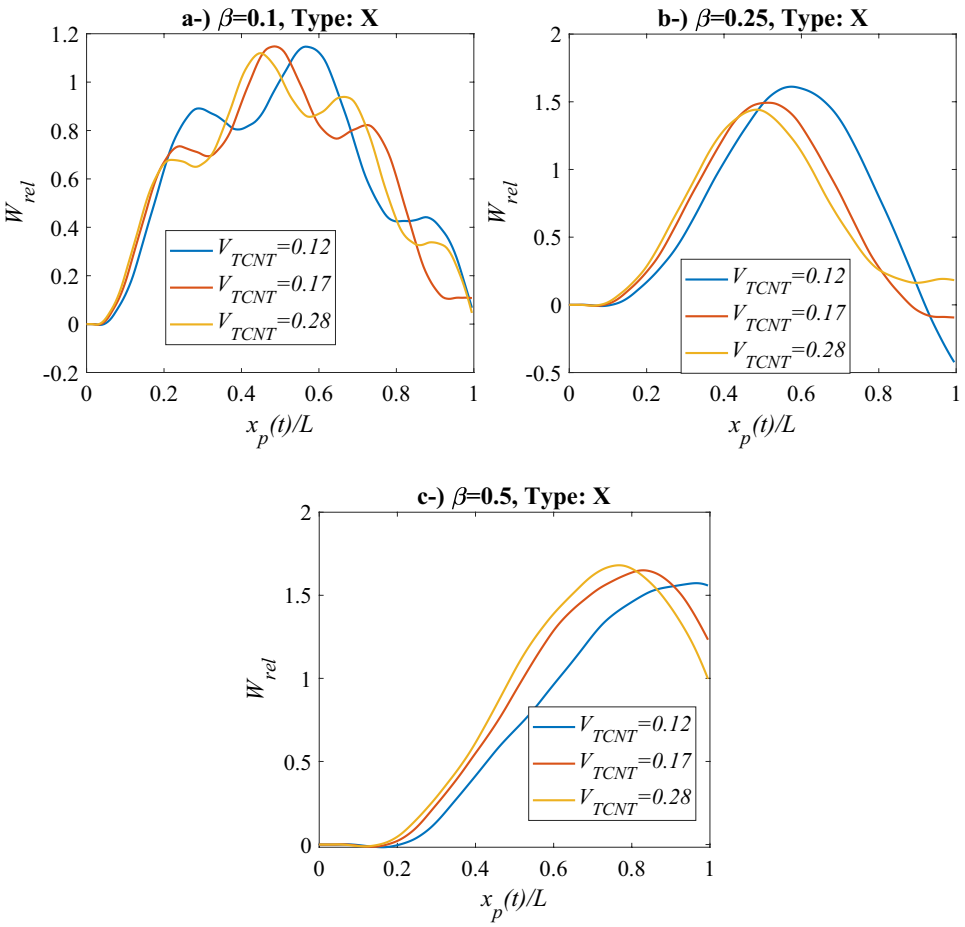

Fig. 8 The comparisons of normalized time histories of the mid-point displacements of FGX-CNT reinforced beams for different total volume fractions$V_{TCNT} = 0.12, 0.17 and 0.28$, and dimensionless velocity of β. **a**$\beta = 0.1$, **b**$\beta = 0.25$, **c** $\beta = 0.5$

create lesser vibration amplitudes for the same load velocities since they are far from the resonance zone. Compared to the resonance velocities of other UD-CNT and FGΛ-CNT reinforced beams, FGX-CNT beams have the highest resonance velocities. In this respect, in the dynamics of FG-CNT reinforced beams, the total volume fractions of CNTs and the distribution of CNTs along the thickness are essential. Thus, in moving load applications, it is possible to design an FG-CNT-reinforced composite beam that can give the best dynamic performance for the mass and speed of the load.

Conclusions

This study models and analyzes the dynamic behavior of FG-CNT-reinforced beams interacting with a moving load. Three types of FG-CNT beams, uniform UD-CNT, FGΛ-CNT, and FGX-CNT composite beams are modeled, and their dynamic behaviors under the moving charge are analyzed. The research findings indicate that the inclusion of CNTs enhances the dynamic behavior of beams, and this improvement grows as the number of CNTs increases. With the addition of CNT, the composite beams behave stronger, and the traveling mass velocity at maximum displacement increases. This also means that using FG-CNT reinforced composite beams for high-speed applications will bring an advantage.

In addition, the distribution of CNTs along the beam thickness is also important besides the total volume fractions of CNTs since the dynamic enhancement of the mixture model type X of the FGX-CNT, in which CNTs are concentrated on the lower and upper surfaces of the beam, is better than the other types. For the same amount of total volume fractions of CNTs, the dynamic behaviors of FGΛ-CNT and UD-CNT beams are close. If a ranking is made for the dynamic behavior of composite beams according to the three types of CNT distributions considered, the FGX-CNT is the best, then FGΛ-CNT, and then UD-CNT. It is observed that the enhancement of the dynamic behavior

of FGΛ-CNT and FGX-CNT beams is weakened when the power-law index k is decreased.

Depending on the type of mixture and the total amount of CNT, the beam with a more flexible structure shows higher displacement at lower speeds than the beams with higher stiffnesses. It is understood from the analysis that the stiffness of the beams increases with the increase in the amount of CNT in all beam types. Using the approach described in this paper, building and evaluating an FG-CNT reinforced composite beam with the appropriate dynamic characteristics for use in an application involving a moving load is feasible.

Data Availability No data was used for the research described in the article.

Declarations

Conflict of Interest The authors declare that they have no known competing financial interests or personal relationships that could have appeared to influence the work reported in this paper.

References

1. Shen H-SS (2009) Nonlinear bending of functionally graded carbon nanotube-reinforced composite plates in thermal environments. Compos Struct 91:9–19. https://doi.org/10.1016/j.compstruct.2009.04.026
2. Bohlén M, Bolton K (2013) Molecular dynamics studies of the influence of single wall carbon nanotubes on the mechanical properties of Poly(vinylidene fluoride). Comput Mater Sci 68:73–80. https://doi.org/10.1016/j.commatsci.2012.10.010
3. Han Y, Elliott J (2007) Molecular dynamics simulations of the elastic properties of polymer/carbon nanotube composites. Comput Mater Sci 39:315–323. https://doi.org/10.1016/j.commatsci.2006.06.011
4. Griebel M, Hamaekers J (2004) Molecular dynamics simulations of the elastic moduli of polymer–carbon nanotube composites. Comput Methods Appl Mech Eng 193:1773–1788. https://doi.org/10.1016/j.cma.2003.12.025
5. Wang CY, Zhang LC (2008) A critical assessment of the elastic properties and effective wall thickness of single-walled carbon nanotubes. Nanotechnology 19:75705. https://doi.org/10.1088/0957-4484/19/7/075705
6. Lu X, Hu Z (2012) Mechanical property evaluation of single-walled carbon nanotubes by finite element modeling. Compos Part B Eng 43:1902–1913. https://doi.org/10.1016/j.compositesb.2012.02.002
7. Giannopoulos GI, Kakavas PA, Anifantis NK (2008) Evaluation of the effective mechanical properties of single walled carbon nanotubes using a spring based finite element approach. Comput Mater Sci 41:561–569. https://doi.org/10.1016/j.commatsci.2007.05.016
8. Yas MH, Samadi N (2012) Free vibrations and buckling analysis of carbon nanotube-reinforced composite Timoshenko beams on elastic foundation. Int J Press Vessel Pip 98:119–128. https://doi.org/10.1016/j.ijpvp.2012.07.012
9. Zhang JF, Zhang XX, Liu ZY, Wang QZ, Xiao BL, Ma ZY (2022) A rigid body dynamics simulation enhanced representative volume element builder for CNT/Al composite. Int J Mech Mater Des 18:407–422. https://doi.org/10.1007/s10999-021-09587-1
10. Lin F, Xiang Y (2014) Vibration of carbon nanotube reinforced composite beams based on the first and third order beam theories. Appl Math Model 38:3741–3754. https://doi.org/10.1016/j.apm.2014.02.008
11. Ansari R, Faghih Shojaei M, Mohammadi V, Gholami R, Sadeghi F (2014) Nonlinear forced vibration analysis of functionally graded carbon nanotube-reinforced composite Timoshenko beams. Compos Struct 113:316–327. https://doi.org/10.1016/j.compstruct.2014.03.015
12. Haghgoo M, Ansari R, Hassanzadeh-Aghdam MK (2022) Analytical-geometrical percolation network model for piezoresistivity of hybrid CNT–CB polymer nanocomposites using Monte Carlo simulations. Int J Mech Mater Des 18:39–61. https://doi.org/10.1007/s10999-021-09568-4
13. Kee J, Kim D, Kim H, Koo J (2023) Enhanced thermal conductivity of polyamide nanocomposites involving expanded graphite–carbon nanotube network structure using supercritical CO2. Adv Compos Mater 00:1–11. https://doi.org/10.1080/09243046.2022.2161479
14. Aydogdu M (2014) On the vibration of aligned carbon nanotube reinforced composite beams. Adv Nano Res 2:199–210. https://doi.org/10.12989/anr.2014.2.4.199
15. Wu HL, Yang J, Kitipornchai S (2016) Nonlinear vibration of functionally graded carbon nanotube-reinforced composite beams with geometric imperfections. Compos Part B Eng 90:86–96. https://doi.org/10.1016/j.compositesb.2015.12.007
16. Shahmohammadi MA, Abdollahi P, Salehipour H (2022) Geometrically nonlinear analysis of doubly curved imperfect shallow shells made of functionally graded carbon nanotube reinforced composite (FG_CNTRC). Mech Based Des Struct Mach 50:3796–3820. https://doi.org/10.1080/15397734.2020.1822182
17. Chaudhari VK, Lal A (2016) Nonlinear free vibration analysis of elastically supported nanotube-reinforced composite beam in thermal environment. Proced. Eng 144:928–935. https://doi.org/10.1016/j.proeng.2016.05.119
18. Saffari PR, Ismail SO, Thongchom C, Sirimontree S, Jearsiripongkul T (2023) Effect of magnetic field on vibration of electrorheological fluid nanoplates with FG-CNTRC layers. J Vib Eng Technol. https://doi.org/10.1007/s42417-023-01048-7
19. Wu H, Kitipornchai S, Yang J (2017) Imperfection sensitivity of thermal post-buckling behaviour of functionally graded carbon nanotube-reinforced composite beams. Appl Math Model 42:735–752. https://doi.org/10.1016/j.apm.2016.10.045
20. Gholami R, Ansari R, Gholami Y (2017) Nonlinear resonant dynamics of geometrically imperfect higher-order shear deformable functionally graded carbon-nanotube reinforced composite beams. Compos Struct 174:45–58. https://doi.org/10.1016/j.compstruct.2017.04.042
21. Shafiei H, Setoodeh AR (2017) Nonlinear free vibration and post-buckling of FG-CNTRC beams on nonlinear foundation. Steel Compos Struct 24:65–77. https://doi.org/10.12989/scs.2017.24.1.065
22. Ghorbani Shenas A, Malekzadeh P, Ziaee S (2017) Vibration analysis of pre-twisted functionally graded carbon nanotube reinforced composite beams in thermal environment. Compos Struct 162:325–340. https://doi.org/10.1016/j.compstruct.2016.12.009
23. Vo-Duy T, Ho-Huu V, Nguyen-Thoi T (2019) Free vibration analysis of laminated FG-CNT reinforced composite beams using finite element method. Front Struct Civ Eng 13:324–336. https://doi.org/10.1007/s11709-018-0466-6
24. Khosravi S, Arvin H, Kiani Y (2019) Vibration analysis of rotating composite beams reinforced with carbon nanotubes in thermal

environment. Int J Mech Sci 164:105187. https://doi.org/10.1016/j.ijmecsci.2019.105187
25. Wu Z, Zhang Y, Yao G, Yang Z (2019) Nonlinear primary and super-harmonic resonances of functionally graded carbon nanotube reinforced composite beams. Int J Mech Sci 153–154:321–340. https://doi.org/10.1016/j.ijmecsci.2019.02.015
26. Taş H, Soykok IF (2019) Effects of carbon nanotube inclusion into the carbon fiber reinforced laminated composites on flexural stiffness: a numerical and theoretical study. Compos Part B Eng 159:44–52. https://doi.org/10.1016/j.compositesb.2018.09.055
27. Talebizadehsardari P, Eyvazian A, Asmael M, Karami B, Shahsavari D, Mahani RB (2020) Static bending analysis of functionally graded polymer composite curved beams reinforced with carbon nanotubes. Thin-Walled Struct 157:107139. https://doi.org/10.1016/j.tws.2020.107139
28. Khosravi S, Arvin H, Kiani Y (2019) Interactive thermal and inertial buckling of rotating temperature-dependent FG-CNT reinforced composite beams. Compos Part B Eng 175:107178. https://doi.org/10.1016/j.compositesb.2019.107178
29. García-Macías E, Guzmán CF, Saavedra Flores EI, Castro-Triguero R (2019) Multiscale modeling of the elastic moduli of CNT-reinforced polymers and fitting of efficiency parameters for the use of the extended rule-of-mixtures. Compos Part B Eng 159:114–131. https://doi.org/10.1016/j.compositesb.2018.09.057
30. Ahmadi M, Ansari R, Hassanzadeh-Aghdam MK (2019) Low velocity impact analysis of beams made of short carbon fiber/carbon nanotube-polymer composite: a hierarchical finite element approach. Mech Adv Mater Struct 26:1104–1114. https://doi.org/10.1080/15376494.2018.1430276
31. Ranjbar M, Feli S (2019) Temperature-dependent analysis of axially functionally graded CNT reinforced micro-cantilever beams subjected to low velocity impact. Mech Adv Mater Struct 26:1154–1168. https://doi.org/10.1080/15376494.2018.1432788
32. Fallah A, Dehkordi MB, Nourbakhsh H, Beni YT (2019) Semi-exact solution for nonlinear dynamic analysis of graded carbon nanotube-reinforced beam with graded shape memory wires. Mech Adv Mater Struct. https://doi.org/10.1080/15376494.2019.1578012
33. Fadaee M, Talebitooti M (2019) Dynamic stability of the rotating carbon nanotube-reinforced adaptive sandwich beams with magnetorheological elastomer core. J Sandw Struct Mater. https://doi.org/10.1177/1099636219849414
34. Palacios JA, Ganesan R (2019) Dynamic response of Carbon-Nanotube-Reinforced-Polymer materials based on multiscale finite element analysis. Compos Part B Eng 166:497–508. https://doi.org/10.1016/j.compositesb.2019.02.039
35. Fu T, Chen Z, Yu H, Wang Z, Liu X (2019) Mechanical behavior of laminated functionally graded carbon nanotube reinforced composite plates resting on elastic foundations in thermal environments. J Compos Mater 53:1159–1179. https://doi.org/10.1177/0021998318796170
36. Kamarian S, Bodaghi M, Isfahani RB, Shakeri M, Yas MH (2021) Influence of carbon nanotubes on thermal expansion coefficient and thermal buckling of polymer composite plates: experimental and numerical investigations. Mech Based Des Struct Mach 49:217–232. https://doi.org/10.1080/15397734.2019.1674664
37. Tran HQ, Vu VT, Tran MT, Nguyen-Tri P (2020) A new four-variable refined plate theory for static analysis of smart laminated functionally graded carbon nanotube reinforced composite plates. Mech Mater 142:103294. https://doi.org/10.1016/j.mechmat.2019.103294
38. Di Sciuva M, Sorrenti M (2019) Bending, free vibration and buckling of functionally graded carbon nanotube-reinforced sandwich plates, using the extended Refined Zigzag Theory. Compos Struct 227:111324. https://doi.org/10.1016/j.compstruct.2019.111324
39. Uspensky B, Avramov K, Derevianko I, Maksymenko-Sheiko K (2023) Vibrations of cylindrical sandwich shell with fused deposition processed honeycomb core and carbon nanotubes reinforced composite faces sheets. J Vib Eng Technol. https://doi.org/10.1007/s42417-023-00960-2
40. Chitour M, Benguediab S, Bouhadra A, Benguediab M, Tounsi A (2023) Effect of variable volume fraction distribution and geometrical parameters on the bending behavior of sandwich plates with FG isotropic face sheets. Mech Based Des Struct Mach. https://doi.org/10.1080/15397734.2023.2197036
41. Van NTH, Hong NT (2023) Novel finite element modeling for free vibration and buckling analysis of non-uniform thickness 2D-FG sandwich porous plates using refined Quasi 3D theory. Mech Based Des Struct Mach. https://doi.org/10.1080/15397734.2023.2197035
42. Bouazza M, Zenkour AM (2020) Vibration of carbon nanotube-reinforced plates via refined nth-higher-order theory. Arch Appl Mech 90:1755–1769. https://doi.org/10.1007/s00419-020-01694-3
43. Adiyaman G (2023) Free vibration analysis of a porous 2D functionally graded beam using a high-order shear deformation theory. J Vib Eng Technol. https://doi.org/10.1007/s42417-023-00996-4
44. Uymaz B, Uymaz G (2023) Three-dimensional thermal vibration of CFFF functionally graded carbon nanotube-reinforced composite plates. J Vib Eng Technol. https://doi.org/10.1007/s42417-023-00957-x
45. Civalek O, Jalaei MH (2020) Shear buckling analysis of functionally graded (FG) carbon nanotube reinforced skew plates with different boundary conditions. Aerosp Sci Technol 99:105753. https://doi.org/10.1016/j.ast.2020.105753
46. Taati E, Borjalilou V, Fallah, and F., Ahmadian, M.T. (2022) On size-dependent nonlinear free vibration of carbon nanotube-reinforced beams based on the nonlocal elasticity theory: Perturbation technique. Mech Based Des Struct Mach 50:2124–2146. https://doi.org/10.1080/15397734.2020.1772087
47. Sobhy M (2019) Levy solution for bending response of FG carbon nanotube reinforced plates under uniform, linear, sinusoidal and exponential distributed loadings. Eng Struct 182:198–212. https://doi.org/10.1016/j.engstruct.2018.12.071
48. Yuan Y, Niu Z, Smitt J (2022) Magneto-hygro-thermal vibration analysis of the viscoelastic nanobeams reinforcedwith carbon nanotubes resting on Kerr's elastic foundation based on NSGT. Adv Compos Mater 00:1–23. https://doi.org/10.1080/09243046.2022.2122766
49. Feli S, Karami L, Jafari SS (2019) Analytical modeling of low velocity impact on carbon nanotube-reinforced composite (CNTRC) plates. Mech Adv Mater Struct 26:394–406. https://doi.org/10.1080/15376494.2017.1400613
50. Vinyas M (2019) A higher-order free vibration analysis of carbon nanotube-reinforced magneto-electro-elastic plates using finite element methods. Compos Part B Eng 158:286–301. https://doi.org/10.1016/j.compositesb.2018.09.086
51. Shen Z, Xia J, Cheng P (2019) Geometrically nonlinear dynamic analysis of FG-CNTRC plates subjected to blast loads using the weak form quadrature element method. Compos Struct 209:775–788. https://doi.org/10.1016/j.compstruct.2018.11.009
52. Ansari R, Torabi J, Hassani R (2019) Thermal buckling analysis of temperature-dependent FG-CNTRC quadrilateral plates. Comput Math with Appl 77:1294–1311. https://doi.org/10.1016/j.camwa.2018.11.009
53. Ansari R, Torabi J, Hassani R (2019) A comprehensive study on the free vibration of arbitrary shaped thick functionally graded

CNT-reinforced composite plates. Eng Struct 181:653–669. https://doi.org/10.1016/j.engstruct.2018.12.049
54. Sharma LK, Grover N, Bhardwaj G (2023) Buckling and Free Vibration Analysis of Temperature-Dependent Functionally Graded CNT-Reinforced Plates. J Vib Eng Technol 11:175–192. https://doi.org/10.1007/s42417-022-00571-3
55. Torabi J, Ansari R, Hassani R (2019) Numerical study on the thermal buckling analysis of CNT-reinforced composite plates with different shapes based on the higher-order shear deformation theory. Eur J Mech-A/Solids 73:144–160. https://doi.org/10.1016/j.euromechsol.2018.07.009
56. Zhou T, Song Y (2019) Three-dimensional nonlinear bending analysis of FG-CNTs reinforced composite plates using the element-free Galerkin method based on the S-R decomposition theorem. Compos Struct 207:519–530. https://doi.org/10.1016/j.compstruct.2018.09.026
57. Koç MA, Esen İ (2017) Modelling and analysis of vehicle-structure-road coupled interaction considering structural flexibility, vehicle parameters and road roughness †. J Mech Sci Technol 31:1–18. https://doi.org/10.1007/s12206-017-0913-y
58. Esen İ, Koç MA (2015) Dynamic response of a 120 mm smooth-bore tank barrel during horizontal and inclined firing positions. Lat Am J Solids Struct 12:1462–1486. https://doi.org/10.1590/1679-78251576
59. Esen İ, Koç MA (2015) Optimization of a passive vibration absorber for a barrel using the genetic algorithm. Expert Syst Appl 42:894–905. https://doi.org/10.1016/j.eswa.2014.08.038
60. Wu J-J (2005) Dynamic analysis of an inclined beam due to moving loads. J Sound Vib 288:107–131. https://doi.org/10.1016/j.jsv.2004.12.020
61. Wu J-J (2008) Transverse and longitudinal vibrations of a frame structure due to a moving trolley and the hoisted object using moving finite element. Int J Mech Sci 50:613–625. https://doi.org/10.1016/j.ijmecsci.2008.02.001
62. Koç MA, Eroğlu M, Esen İ (2022) Dynamic analysis of high-speed train moving on perforated Timoshenko and Euler-Bernoulli beams. Int J Mech Mater Des. https://doi.org/10.1007/s10999-022-09610-z
63. Baek S (2022) Dynamic response predictions of frictionally constrained lap joints subjected to cyclic loading. Int J Mech Mater Des 18:491–507. https://doi.org/10.1007/s10999-021-09580-8
64. Wang Y, Zhou A, Fu T, Zhang W (2020) Transient response of a sandwich beam with functionally graded porous core traversed by a non-uniformly distributed moving mass. Int J Mech Mater Des 16:519–540. https://doi.org/10.1007/s10999-019-09483-9
65. Shi P (2022) Three-dimensional isogeometric analysis of functionally graded carbon nanotube-reinforced composite plates. Arch Appl Mech 92:3033–3063. https://doi.org/10.1007/s00419-022-02224-z
66. Chiker Y, Bachene M, Bouaziz S, Guemana M, Amar MB, Haddar M (2021) Free vibration analysis of hybrid laminated plates containing multilayer functionally graded carbon nanotube-reinforced composite plies using a layer-wise formulation. Arch Appl Mech 91:463–485. https://doi.org/10.1007/s00419-020-01783-3
67. Zhou L (2022) Predicting natural frequency of functionally graded CNT-reinforced composite cylinders in similitude. Arch Appl Mech 92:3781–3800. https://doi.org/10.1007/s00419-022-02262-7
68. Özmen R, Kılıç R, Esen I (2022) Thermomechanical vibration and buckling response of nonlocal strain gradient porous FG nanobeams subjected to magnetic and thermal fields. Mech Adv Mater Struct. https://doi.org/10.1080/15376494.2022.2124000
69. Li L, Hu Y (2016) Nonlinear bending and free vibration analyses of nonlocal strain gradient beams made of functionally graded material. Int J Eng Sci 107:77–97. https://doi.org/10.1016/j.ijengsci.2016.07.011
70. Lim CW, Zhang G, Reddy JN (2015) A higher-order nonlocal elasticity and strain gradient theory and its applications in wave propagation. J Mech Phys Solids 78:298–313. https://doi.org/10.1016/j.jmps.2015.02.001
71. Reddy JN (2007) Nonlocal theories for bending, buckling and vibration of beams. Int J Eng Sci 45:288–307. https://doi.org/10.1016/j.ijengsci.2007.04.004
72. Nguyen DK, Gan BS, Le TH (2013) Dynamic response of non-uniform functionally graded beams subjected to a variable speed moving load. J Comput Sci Technol 7:12–27. https://doi.org/10.1299/jcst.7.12
73. Sina SA, Navazi HM, Haddadpour H (2009) An analytical method for free vibration analysis of functionally graded beams. Mater Des 30:741–747. https://doi.org/10.1016/j.matdes.2008.05.015
74. Esen I (2019) Dynamic response of a functionally graded Timoshenko beam on two-parameter elastic foundations due to a variable velocity moving mass. Int J Mech Sci 153–154:21–35. https://doi.org/10.1016/j.ijmecsci.2019.01.033
75. Şimşek M, Kocatürk T (2009) Free and forced vibration of a functionally graded beam subjected to a concentrated moving harmonic load. Compos Struct 90:465–473. https://doi.org/10.1016/j.compstruct.2009.04.024
76. Khalili SMR, Jafari AA, Eftekhari SA (2010) A mixed Ritz-DQ method for forced vibration of functionally graded beams carrying moving loads. Compos Struct 92:2497–2511. https://doi.org/10.1016/j.compstruct.2010.02.012
77. Shen HS, Xiang Y (2012) Nonlinear vibration of nanotube-reinforced composite cylindrical shells in thermal environments. Comput Methods Appl Mech Eng 213–216:196–205. https://doi.org/10.1016/j.cma.2011.11.025
78. Fryba L (1999) Vibration solids and structures under moving loads. Thomas Telford House
79. Oguamanam DCD, Hansen JS, Heppler GR (1998) Dynamic response of an overhead crane system. J Sound Vib 213:889–906. https://doi.org/10.1006/jsvi.1998.1564
80. Oguamanam DCD, Hansen JS, Heppler GR (2001) Dynamics of a three-dimensional overhead crane system. J Sound Vib 242:411–426. https://doi.org/10.1006/jsvi.2000.3375